Extended field of view soft x-ray Fourier transform holography: toward imaging ultrafast evolution in a single shot

William F. Schlotter,[1,2,*] Jan Lüning,[3,4,2] Ramon Rick,[1,2] Kang Chen,[1,2] Andreas Scherz,[2] Stefan Eisebitt,[5] Christian M. Günther,[5] Wolfgang Eberhardt,[5] Olav Hellwig,[6,5] and Joachim Stöhr[2]

[1]*Department of Applied Physics, 316 Via Pueblo Mall, Stanford University, Stanford, California 94305, USA*
[2]*Stanford Synchrotron Radiation Laboratory, SLAC, Menlo Park, California 94025, USA*
[3]*LCP-MR Université Pierre et Marie Curie, 11 Rue Pierre et Marie Curie, 75005 Paris, France*
[4]*Synchrotron SOLEIL, L'Orme des Merisiers, Saint-Aubin - BP 48, 91192 Gif-sur-Yvette, France*
[5]*BESSY m.b.H., Albert-Einstein-Straße 15, 12489 Berlin, Germany*
[6]*San Jose Research Center, Hitachi Global Storage Technologies, 3403 Yerba Buena Road, California 95135, USA*
**Corresponding author: wschlott@stanford.edu*

Received April 30, 2007; revised July 4, 2007; accepted August 5, 2007;
posted September 28, 2007 (Doc. ID 82552); published October 19, 2007

Panoramic full-field imaging is demonstrated by applying spatial multiplexing to Fourier transform holography. Multiple object and reference waves extend the effective field of view for lensless imaging without compromising the spatial resolution. In this way, local regions of interest distributed throughout a sample can be simultaneously imaged with high spatial resolution. A method is proposed for capturing multiple ultrafast images of a sample with a single x-ray pulse. © 2007 Optical Society of America

OCIS codes: 180.7640, 090.4220, 320.2250.

Lensless Fourier transform holography (FTH) is an imaging technique well suited for high resolution x-ray microscopy [1–5]. In FTH the reference and object waves originate from adjacent sites on the scattering plane which is perpendicular to the optical axis. When the scattering plane is illuminated by a coherent wavefront, interference between the object and reference waves are detected in the far field as fringes which form a hologram. The two-dimensional (2D) Fourier transform of this hologram is the autocorrelation of the two waves in the scattering plane and thus contains a reconstructed real space image of the object. Because the image is the convolution of the reference and object wave amplitudes, a delta function-like reference is desired for high spatial resolution, and a large object profile is preferred for a wide field of view. Realizing high spatial resolution requires a large numerical aperture for the hologram. However, a large object generates high spatial frequency fringes in the hologram, which must be resolved by the detector pixels to successfully reconstruct the entire field of view. This balance is characteristic of full-field imaging, where the field of view and spatial resolution are competing quantities. However, by using multiple object and reference signals, the effective field of view can be extended without compromising the numerical aperture of the detected hologram [6].

Here we demonstrate multiple object FTH at soft x-ray wavelengths which allows us to simultaneously record images of isolated areas on a sample. We show that this method is capable of imaging local areas of a sample with high spatial resolution, and envision its application to record images of ultrafast processes by combining it with a cross-beam pump probe illumination.

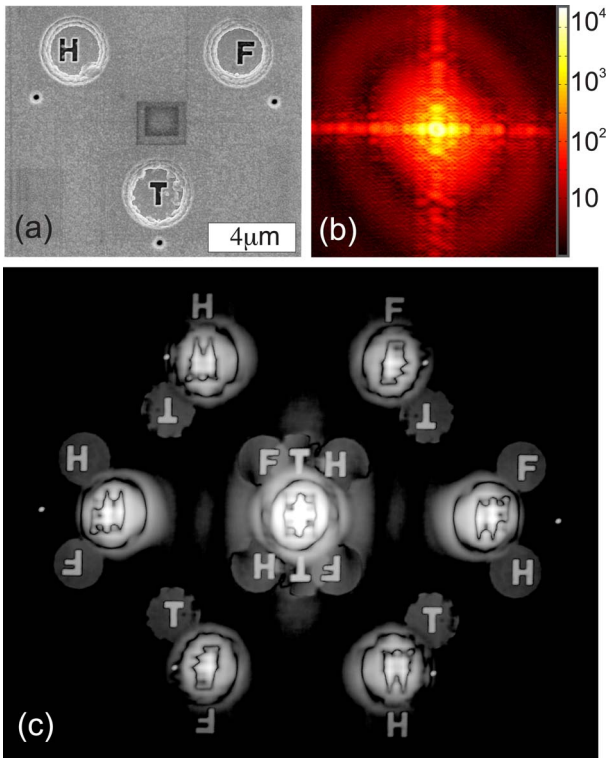

Fig. 1. (Color online) (a) SEM of the FTH transmission mask. An x-ray opaque 1.4 μm Au layer was sputter deposited onto a 100 nm Si_3N_4 membrane. (b) The soft x-ray Fourier transform hologram shown was recorded with a momentum transfer range of $q = \pm 0.09\ \mathrm{nm}^{-1}$. The base ten logarithm of the intensity is shown in false color with the number of photons detected specified by the colorbar. (c) The squared magnitude of the spatial Fourier transform of the hologram in (b) is the autocorrelation reconstruction that presents the intensity transmission profile of the sample.

The methodology for acquiring high resolution images of specific regions on a sample is introduced with the transmission mask structure shown in Fig. 1(a). The Au nanostructure is composed of three circular isolated regions of interest each containing a block letter shaped structure with an intensity transmittance of 12% at $\lambda = 1.58$ nm. The focused ion beam (FIB) fabrication techniques for this structure were recently reported for a similar sample [7]. The 120 $\times$ 160 nm elliptical reference holes have unity transmittance and are strategically placed adjacent to the letters.

To record the coherent diffraction pattern displayed in Fig. 1(b), the sample was illuminated with a properly filtered soft x-ray beam originating from an undulator source. The wavelength for the experiment, $\lambda = 1.58$ nm, was selected by a spherical grating monochromator with energy resolution, $\lambda/\Delta\lambda > 5000$, thus providing a longitudinal coherence length, $\xi_l = \lambda^2/(2\Delta\lambda) > 4\ \mu$m, sufficient for interference. After spatial filtering the transverse coherence width of the beam incident on the sample was $\xi_t > 20\ \mu$m. The pattern was recorded with an in-vacuum, back side illuminated, thermoelectrically cooled CCD camera [8].

The interference fringes formed by scattering from the longest length scales on the sample (11 μm) were resolved on the detector because the spatial periodicity of these fringes exceeded the CCD pixel pitch, which defines the detected momentum transfer increment of the hologram q_{inc}. For the hologram in Fig. 1(b) $q_{\mathrm{inc}} = 0.15\ \mu\mathrm{m}^{-1}$. As a result the Fourier transform reconstruction, Fig. 1(c), contains the autocorrelation of all scattering structures. In particular, the block letters appear as "FTH" above and below the center of the reconstruction, due to the strategic reference hole placement. Therefore by augmenting the detected q and thus undersampling the coherent diffraction pattern it is possible to realize additional spatial resolution without sacrificing field of view information for the isolated regions.

The key to extending the effective field of view is the strategic arrangement of each reference hole with respect to the neighboring object region. Images of the isolated regions should tile, not overlap, in the autocorrelation [6,7]. Furthermore, for the highest spatial resolution, the reconstructed field of view should be matched to the extent of the largest local region on the sample. Since these requirements are compatible with single shot illumination from a pulsed x-ray source, isolated regions on a sample can be imaged with a single pulse.

We further extend the field of view with the transmission mask illustrated in Fig. 2(a). This nanostructured Au absorption mask contains 40 nm features spanning 180 μm. The scanning electron microscopy (SEM) image in Fig. 2(b) shows one of the four arrow-shaped object and reference pairs that spans the distance $\Delta_{ro} = 6.1\ \mu$m. Both the reference and the arrow were milled through 1.0 μm of Au and 100 nm of Si_3N_4 using the FIB and thus have unity transmission.

The coherent diffraction pattern displayed in Fig. 2(c) was recorded at $\lambda = 1.56$ nm with $\xi_l > 4\ \mu$m. For this experiment the transverse coherence width $\xi_t > 10\ \mu$m did not span the spacing between local sample regions, and the reconstructed field of view was matched to the local length scales on the sample (e.g., Δ_{ro}). As a result the coherent diffraction pattern shown in Fig. 2(c) contains only the superposition of the four independent holograms which were recorded concurrently. All four of the arrows are clearly visible in Fig. 2(d), which displays the squared magnitude of

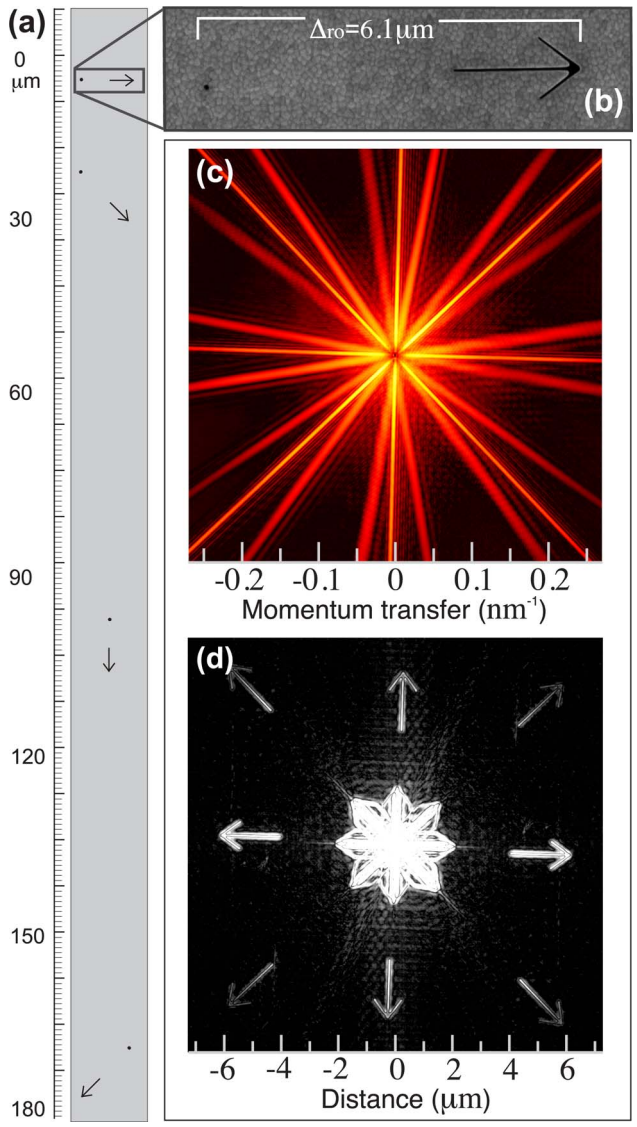

Fig. 2. (Color online) (a) Scale illustration of the extended field of view absorption mask spanning 180 μm. Transmission structures appear black while the opaque Au is gray. (b) SEM of an isolated region of the illustration is enlarged, displaying both a ~70 nm diameter reference hole and arrow structure. (c) The hologram is a composite of data recorded with and without a beamstop. To cope with the direct beam a Gaussian high pass filter was applied to the hologram thus minimizing the ringing in the reconstruction as suggested by Chapman *et al.* [12]. (d) Fourier transform reconstruction of the hologram where the <50 nm spatial resolution is limited by the size of the reference. The weak contrast in the diagonal arrows results from reduced high frequency fringe visibility. One possible source is the presence of charge in multiple adjacent CCD pixels upon detection of a single photon.

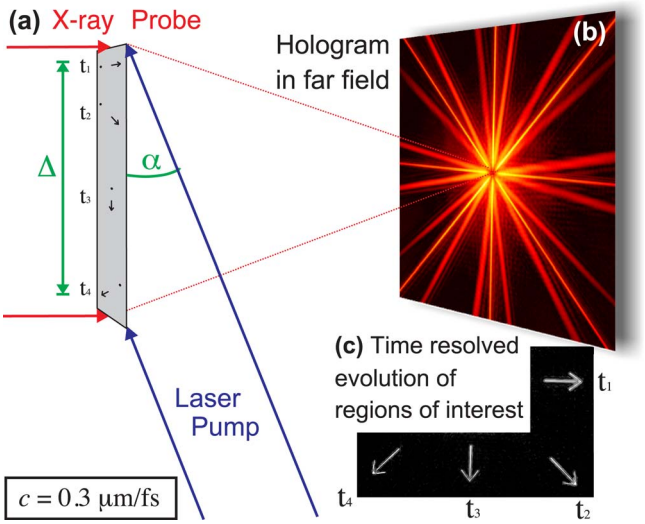

Fig. 3. (Color online) Illustration of the envisioned cross-beam time resolved single shot imaging experiment. (a) The pump pulse propagates along the sample to excite it and establish time scale $t_x=(\Delta \cos \alpha)/c$. (b) The x-ray probe pulse simultaneously illuminates the entire sample thus storing the temporal evolution of the sample in the hologram. (c) The relative delay between the pump and probe is defined by each arrow's orientation. The horizontal arrow, t_1, has the shortest delay and t_4 the longest (the contrast in this image has been enhanced for clarity).

the 2D Fourier transform of the hologram in Fig. 2(b). We note that this is similar to multiple exposure holography, which has been studied at visible wavelengths [9].

The ability to precisely capture ultrafast temporal evolution across a single spatial dimension can be realized with a cross-beam pump probe experimental geometry [10,11]. Such a configuration is illustrated in Fig. 3, where an ultrafast optical pump pulse with incidence angle α excites the samples separated by Δ. The evolution of the system is captured by a subsequent probe pulse from an ultrafast x-ray source at normal incidence. Since the entire mask is simultaneously illuminated by the x-ray probe pulse, the resulting hologram contains instantaneous diffraction patterns from each position along the sample and their respective temporal delays. This temporal evolution would be visible in the Fourier transform reconstruction of the scattering pattern shown in Fig. 3(c). In the illustrated geometry the arrows function as the hand on an ultrafast clock, pointing toward a given time delay, t_x. Longer delays result when α is small, with the longest possible delay set by the transverse width of the x-ray probe pulse.

The key feature of applying FTH to a cross-beam geometry is the achievable temporal resolution of the time delay t_x. Since t_x is calculated from Δ, higher spatial resolution implies improved temporal precision. The spatial resolution in FTH is set by the size of the reference aperture, therefore femtosecond temporal precision is viable. However, this geometrically calculable temporal precision may be limited by the pulse duration. Since the image is detected by the probe pulse its duration defines the temporal uncertainty. Additionally, depending on the experiment and geometry the rising edge and duration of the pump pulse may also augment the temporal uncertainty.

In conclusion, we have demonstrated a method for an effective extension of the field of view for FTH. Remarkably, isolated regions distributed about a sample can be imaged simultaneously without compromising spatial resolution. An experimental geometry applicable to ultrafast single shot imaging was suggested that is especially relevant in light of experiments planned for x-ray lasers.

The program of the Stanford authors is supported by the Office of Basic Energy Sciences, U.S. Department of Energy (BES-DoE). These experiments were carried out on beamline UE52-SGM at BESSY and beamline 5-2 at SSRL. SSRL is a national user facility operated by Stanford University on behalf of BES-DoE. The authors thank H. Zabel for making available the ALICE scattering chamber at BESSY.

References

1. G. W. Stroke and D. Falconer, Phys. Lett. **13**, 306 (1964).
2. J. T. Winthrop and C. R. Worthington, Phys. Lett. **15**, 124 (1965).
3. I. McNulty, J. Kirz, C. Jacobsen, E. H. Anderson, M. R. Howells, and D. P. Kern, Science **256**, 1009 (1992).
4. S. Eisebitt, J. Lüning, W. F. Schlotter, M. Lörgen, O. Hellwig, W. Eberhardt, and J. Stöhr, Nature **432**, 885 (2004).
5. H. He, U. Weierstall, J. C. H. Spence, H. A. M. Howells, H. Padmore, S. Marchesini, and H. N. Chapman, Appl. Phys. Lett. **85**, 2454 (2004).
6. J. W. Goodman and J. D. Gaskill, Proc. IEEE **57**, 823 (1969).
7. W. F. Schlotter, R. Rick, K. Chen, A. Scherz, J. Stöhr, J. Lüning, S. Eisebitt, C. Günther, W. Eberhardt, O. Hellwig, and I. McNulty, Appl. Phys. Lett. **89**, 163112 (2006).
8. Princeton Instruments Camera models PI-SX and PI-MTE.
9. R. W. Stroud and W. T. Rhodes, Appl. Opt. **33**, 3627 (1994).
10. R. Neutze and J. Hajdu, Proc. Natl. Acad. Sci. U.S.A. **94**, 5651 (1997).
11. O. Synnergren, M. Harbst, T. Missalla, J. Larsson, G. Katona, R. Neutze, and R. Wouts, Appl. Phys. Lett. **80**, 3727 (2002).
12. H. N. Chapman, A. Barty, S. Marchesini, A. Noy, S. R. Hau-Riege, C. Cui, M. R. Howells, R. Rosen, H. He, J. C. H. Spence, U. Weierstall, T. Beetz, C. Jacobsen, and D. Shapiro, J. Opt. Soc. Am. A **23**, 1179 (2006).